Journal of Applied Polymer Science

Thermomechanical Properties of Poly(lactic acid) Films Reinforced with Hydroxyapatite and Regenerated Cellulose Microfibers

Arman Mahboubi Soufiani,[1] Masoud Salehi,[1] Mikael Skrifvars,[1] Maria Persson,[2] Sung-Woo Cho[3]

[1]School of Engineering, University of Borås, S-501 90 Borås, Sweden

[2]Department of Anatomy and Cell Biology, University of Oulu, FIN-90014 Oulu, Finland

[3]ABB AB, Corporate Research, 721 78 Västerås, Sweden

Correspondence to: M. Skrifvars (E-mail: mikael.skrifvars@hb.se)

ABSTRACT: Novel composite films constituted of poly(lactic acid) (PLA), hydroxyapatite (HAp), and two types of regenerated cellulose fillers—particulate and fibrous type—were produced by melt extrusion in a twin-screw micro-compounder. The effect of the film composition on the tensile and dynamic mechanical behavior and the HAp dispersion in the PLA matrix were investigated thoroughly. Appearance of crazed regions and prevention of HAp aggregation in the PLA matrix were elucidated in the composites with up to 15 wt % particulate cellulose content, which was the main reason for only slight reduction in the tensile properties, and consequently trivial degradation of their pre-failure energy absorption as compared to neat PLA films. Superior dynamical energy storage capacities were obtained for the particulate cellulose modified composites, while their fibrous counterparts had not as good properties. Additionally, the anisotropic mechanical behavior obtained for the extruded composites should be favorable for use as biomaterials aimed at bone tissue engineering applications. © 2014 Wiley Periodicals, Inc. J. Appl. Polym. Sci. **2014**, *131*, 40911.

KEYWORDS: biomaterials; cellulose and other wood products; films; mechanical properties; thermal properties

Received 13 November 2013; accepted 23 April 2014

DOI: 10.1002/app.40911

INTRODUCTION

Poly(lactic acid) (PLA) has been widely used in medical implants in the form of screw, plates, pins, and rods for the healing of bone fractures. There are several advantages when using PLA in these applications. Under physiological conditions, PLA degrades into lactic acid within 6 months to 2 years, and thus there is no need for additional operations to remove the implant.[1,2] In the case of metallic bone implants, the main challenge is stress shielding, which means the reduction of bone density and strength due to the lack of normal stress imposed on the bone tissue, as the metallic implant carries the load. Biopolymer implants, such as PLA, do not necessarily cause stress shielding, if the mechanical strength of biopolymer is compatible to the natural bone strength. The mechanical properties and the physiological degradation of PLA can be regulated by variation in the stereochemical composition and by copolymerization with other hydroxyacids. This is an evident benefit compared to natural polymers such as chitin, alginate, or collagen, which are rather complex macromolecules with properties difficult to control.[3] PLA possesses however, some properties, which are challenging in biomedical and tissue engineering applications. Of these, deficiency in biological signaling present in natural extra cellular matrix, low wettability, autocatalytic hydrolysis leading to decrease in pH, as well as suppression of the mechanical properties under physiological conditions can be stated.[3–6] Therefore, modification of PLA by addition of reinforcements has been applied to overcome these shortcomings.[7] By the addition of reinforcements it is possible to tailor the mechanical properties, if there is an efficient stress transfer from the PLA matrix to the reinforcement. Cellulose has a well proven compatibility with biological soft and hard tissues.[8] The native cellulose can be transformed to regenerated cellulose fibers, by dissolving in various organic solvents or ionic liquids, after which the cellulose fiber is regenerated by coagulation in a non-solvent, after passing through a spinneret.[9] Regenerated cellulose fibers have properties which are of interest in many applications, such as high elongation at break,[9] uniform filament dimensions, high purity, even quality, as well as reproducible mechanical properties.[10] They have additionally several characteristics important for biomedical applications, such as biocompatibility, non-toxicity, and high mechanical strength in wet environments.[11] The biodegradation of regenerated cellulose scaffolds to glucose has also been proven to occur under physiological conditions by an enzymatic process.[12]

Hydroxyapatite (HAp) is a well-known bioactive mineral, which can enhance the osteoconductivity of PLA and other

biopolymers, thus HAp is used in bone cell tissue engineering applications. The activity is based on direct bonding of the phosphate to the human bone tissue and induce pH stabilization of the physiological environment during *in vivo* biodegradation of the substrate.[6,13] HAp also has a high affinity for proteins due to the effect on surface morphology of the substrate which facilitates protein adsorption on the biomaterial substrate.[14] Furthermore, the combination of cellulosic reinforcements and bioactive phosphates in a variety of biopolymers has been evaluated for *in vivo* and *in vitro* tissue engineering applications.[8,11,15–17] The incorporation of nanosize HAp into the cellulose matrix has been shown to give strength enhancement and reduction of the composites elongation at break.[14] It has also been shown that scaffolds filled with nanosize HAp demonstrate higher compressive modulus and protein adsorption capability when compared with PLA modified with microsize HAp.[18]

Many reviews have covered the chemical, physical, and biological characteristics of biomaterials currently of high interest for tissue engineering applications, particularly those relevant to bone reconstruction.[5,6,19–21] For tissue engineering scaffolds, the shape, porosity, surface area as well as surface characteristics, are critical factors. The scaffold fabrication is also important, especially regarding the possibility to combine different active materials in one manufacturing process, and to facilitate the scaffolds' structure–property relationship.[1,22] Foaming, freeze-drying, solvent casting, phase separation, and electrospinning are some common methods to produce porous scaffolds with large surface area. To be able to determine the most suitable material constituents for a scaffold or a bone implant, it is necessary to perform testing and characterization regarding mechanical and physical properties, processing parameters as well as evaluations regarding its cytotoxicity, cell attachment, and biocompatibility. For this purpose, it is often much easier and timesaving to prepare model-substrates such as films with the same composition as the scaffold or implant.

Based on the literature, it is evident that biocomposites composed of PLA, bioactive phosphates such as HAp, and regenerated cellulose could provide interesting opportunities in the development of novel bioactive materials for bone tissue engineering scaffolds and bone implants.[3,6] The aim of this study is to evaluate the mechanical and viscoelastic characteristics of melt-extruded PLA/HAp/cellulose biocomposite films, with the purpose to find an optimal composition which could be suitable for the fabrication of tissue engineering scaffolds and bone implants. Film extrusion was selected as the processing method, as it is a rather straightforward procedure to make reproducible material specimens, which can be characterized regarding mechanical and thermal properties, processing and fabrication aspects, as well as cell culture tests. A main challenge in composites is to achieve uniform distribution of the fillers and reinforcements in the matrix, so we used a solvent blending process to overcome this aspect. Two types of regenerated cellulose, a particle type and a fibrous type, were studied to investigate the effect of cellulose morphology on the properties. The purpose of using two morphologically different cellulose types was initially to assess their influence on the mechanical properties of the composites. As bioactive phosphate, we used nanosize hydroxyapatite, and we wanted to investigate the HAp particle distribution in the composite films. The surface morphology of the extruded films was also studied, which is of interest as it is known that a rough surface facilitates the enhancement of protein adsorption and anchoring, which are important factors in tissue engineering applications.[23] The hypothesis was that the HAp and cellulose in the form of particles or short fibers would give a surface morphology favorable for tissue engineering. This has been shown for mesenchymal stem cells, which are able to sense the surface physical properties such as stiffness, roughness, topography, and/or texture.[3] Although the effect of microroughness is still controversial concerning their capability in cell proliferation, it is presumed that textured surfaces facilitate protein adsorption and increase the initial attachment of the cells.[23]

To the best of our knowledge, this is the first time the effect of variation in morphology and concentration of regenerated cellulose on the mechanical and thermal properties of PLA/HAp composites produced by melt film extrusion is investigated. After confirmation of the properties, scaffold could be made from the most promising compositions, by various techniques. By melt- or electrospinning it is possible to prepare filaments and yarns which are converted into porous textile structures, which can function as scaffolds. It could also be possible to prepare porous structures by foaming or the films could be used as such as a cell growth substrate. This will be the scope for further investigations.

EXPERIMENTAL

Materials

PLA 6201D with density of 1.24 kg m^{-3} was kindly provided by NatureWorks®. Hydroxyapatite with a particle size less than 200 nm, a surface area of 9.4 m^2 g^{-1}, and a density of 3.85 ± 0.17 kg m^{-3} was purchased from Sigma Aldrich. Two morphologically different types of regenerated cellulose were used; a particle type cellulose (Tencel CP 12) with average diameter of 12 μm and fibrous cellulose (Tencel FCP 10/400) with average fiber diameter of 10 μm, and length of 400 μm. Both were supplied by Lenzing AG, Austria. The densities of the fibrous cellulose (named shortly as FCP) and the particle cellulose (named shortly as CP) were measured to be 1.56 and 1.51 g m^{-3}, respectively. Analytical reagent grade of 1,4-dioxane with 99.99% purity was used to dissolve the PLA, this was purchased from Fisher Chemical, UK. Paraffin wax 76243 of analytical grade was purchased from Fluka with experimentally measured density of around 0.908 g m^{-3}.

Blend Preparation

Before the film extrusion, PLA was blended with 10 wt % HAp and various amounts of cellulose to get compounds with 1, 3, 5, 7, 10, 15, and 20 wt % cellulose content related to the PLA amount, as shown in Table I. The maximum cellulose content was 20 wt %, as a higher content was expected to give composites with rather poor properties due to difficulties to get homogeneous compounds. This was also verified in our preliminary compounding tests. A solvent dilution method was used to obtain homogeneous composition for all blends. The proper amount of the cellulose and the HAp was first mixed with 450 g (435 mL) 1,4-dioxane at room temperature for 4 h to obtain

Table I. Composite Film Compositions

	Masterbatch constituents		
Sample	PLA (g)	HAp (g)	Cellulose/ FCP (g)
PLA/HAp	40.91	4.09	-
PLA/HAp/FCP1	40.54	4.05	0.41
PLA/HAp/FCP3	39.82	3.98	1.20
PLA/HAp/FCP5	39.13	3.91	1.96
PLA/HAp/FCP7	38.46	3.85	2.69
PLA/HAp/FCP10	37.50	3.75	3.75
PLA/HAp/FCP15	36.00	3.60	5.40
PLA/HAp/FCP20	34.62	3.46	6.92

The fibrous cellulose (FCP) content in wt % related to PLA amount is given by the number in the sample name. The exact same formulation is used for the particulate cellulose (CP) containing composite films. The total masterbatch weight was 45 g, which was dissolved in 450 g dioxane. In all films, the HAp content is 10 wt % related to PLA amount.

homogeneous slurry. Then 40 g PLA was added, and the mixture was kept under stirring for additional 12 h at 25°C until the PLA was fully dissolved. The solution was then drop-wise added to a flask containing liquid nitrogen to form solid composite granulates. By this very rapid quenching it is ensured that the cellulose and the HAp are homogeneous distributed in the PLA matrix. The obtained granulates were freeze-dried for 24 h and finally oven-dried at 50°C for 24 h to evaporate any residual dioxane, rendering non-toxic granulates, which is essential for further cell cultivation. The granulates were stored under dry conditions, to prevent possible humidity uptake, and further PLA degradation. Using this solvent dilution method, it is possible to ensure proper dispersion of the HAp and the cellulose in the PLA matrix, which will facilitate a homogeneous film extrusion and prevent possible thermal and mechanical degradation of the polymer matrix during the compounding.

Film Extrusion

The films were produced in a lab-scale twin-screw micro-compounder (15cc DSM Xplore®, the Netherlands), equipped with a film extrusion die (0.4-mm thick and 25-mm wide) and rotating film-uptake rolls. The extrusion parameters were selected based on extrusion pre-trials where the conditions to obtain optimal and even film quality were examined. The extrusion was done at constant mixing time (5 min), temperature (195°C) and rotational speed (50 rpm), and using a die temperature of 180°C. By running the micro-compounder under force control set to 950–1000 N it was possible to obtain films with uniform film thickness. The extruded films were formed by air flow cooling after the die, and further collected on a rotating roll, with a take-up speed equal to the speed for the film extruding through the die. The final film thickness was measured by a micrometer at several points of the film during the extrusion.

CHARACTERIZATION

Thermogravimetric Analysis

Thermogravimetric analysis (TGA) was done in a Q500 TGA from TA Instruments, and by heating from room temperature to 700°C with a 10°C min^{-1} heating ramp under nitrogen with flow rate of 50 mL min^{-1}. Samples were randomly taken from different positions along the extruded composite films; the starting part, the middle part, and the finishing part, and from each part one sample was taken in the middle of the film, and one from the outer edge. Totally, this gave six TGA samples, three representing the middle part of the film, and three representing the edge part of the film. The gravimetric distribution of the HAp was determined by comparing the average temperatures at which 5% (T_5) respective 80% (T_{80}) weight loss occur, and by detecting the residual char content at 700°C. Samples were not dried prior to the TGA measurements, and thus a slight drop in the TGA signal at 100°C was observed for all the samples. This will not however affect the determination of the gravimetric amount of HAp in the films.

Scanning Electron Microscopy

The morphology of the composite films was examined with a table-top scanning electron microscope (TM-1000, Hitachi, Japan). Prior to scanning electron microscopy (SEM) analysis, the tensile-fractured cross-sections of the samples were mounted on a metal stub and stored in a Denton vacuum under 0.1 mbar vacuum pressure. The test specimens were then coated for about 30 s with a Gold powder layer (~10 nm) using an Agar high-resolution sputter coater (model 208RH), equipped with a gold target/Agar thickness monitor controller. The SEM analysis was performed on low vacuum mode (LV-SEM) to take micrographs at various magnifications. The instrument uses an electron beam accelerated at 15 kV.

Differential Scanning Calorimetry

The thermal characteristics were measured in a Q1000 DSC from TA® Instruments. Degree of crystallinity, glass transition, cold crystallization, and melting temperatures as well as their corresponding endothermic and/or exothermic enthalpies were determined from three replicated samples of the neat PLA and the made composite films. The first heating cycle was from 25 to 210°C with 10°C min^{-1} temperature ramp, after which the sample was cooled to 25°C with 5°C min^{-1} rate, before the final heating to 210°C as for the first scan. The analysis was done under nitrogen with a flow rate of 50 mL min^{-1}. The crystallinity of the samples was calculated according to the following relation,[24–30] based on the heat released by formation and required during the melting process of the crystals taking into account the weight contribution from the fillers:

$$\chi_c\% = \frac{\Delta H_m - \Delta H_{cc}}{\varnothing \times \Delta H_m^0} \quad (1)$$

where χ_c% is normalized degree of crystallinity of PLA and ΔH_m, ΔH_{cc}, and $\varnothing$ are the melting enthalpy (J g^{-1}) and cold-crystallization enthalpy of the composites (J g^{-1}) and the weight percentage of the PLA in the composites (%), respectively. For ΔH_m^0, the value 93 J g^{-1} [24,25,29] was used in this study, which is the melting enthalpy of a pure 100% crystalline PLA.

Tensile Testing

Prior to the mechanical testing, the films were conditioned for 48 h at 23°C and 50% relative humidity in a Memmert HPP108

Table II. Thermogravimetric Analysis of Extruded Films

Sample	T_5 at EP (°C)	T_5 at MP (°C)	T_{80} at EP (°C)	T_{80} at MP (°C)	Char residue at EP (wt %)	Char residue at MP (wt %)
PLA/Hap	291.7 ± 2.2	297.8 ± 6.1	343.5 ± 2.4	344.9 ± 4.4	9.3 ± 0.2	9.2 ± 0.2
PLA/HAp/CP3	276.6 ± 1.5	274.2 ± 3.2	335.0 ± 0.4	335.9 ± 1.4	9.5 ± 0.1	9.5 ± 0.1
PLA/HAp/FCP3	287.8 ± 2.6	286.0 ± 1.3	340.8 ± 1.3	340.1 ± 0.4	9.1 ± 0.4	9.5 ± 0.0
PLA/HAp/CP10	284.8 ± 3.2	280.6 ± 4.4	343.8 ± 2.7	341.6 ± 0.6	9.7 ± 0.1	9.7 ± 0.1
PLA/HAp/FCP10	286.3 ± 0.3	286.1 ± 1.1	341.5 ± 0.9	341.1 ± 4.1	9.8 ± 0.1	9.9 ± 0.1
PLA/HAp/CP20	292.1 ± 2.4	285.5 ± 6.2	350.6 ± 0.9	351.2 ± 1.0	9.1 ± 1.0	9.5 ± 0.1
PLA/HAp/FCP20	271.9 ± 2.1	272.3 ± 3.6	339.8 ± 0.8	339.5 ± 1.0	10.2 ± 0.1	10.2 ± 0.1

Temperatures for 5 wt % (T_5) respective 80 wt % (T_{80}) weight loss and the char residue at 700°C for samples taken at the film edge (EP) and at middle (MP) point of film are given. The average values are calculated from three replicate samples taken from the film at edge and middle point.

conditioning oven, according to DIN EN ISO 291. Dumbbell-shape specimens were press cut from the films by an Elastocon EP08 cutter. The films (length 75 mm, width 3.97 mm, and thickness of about 400 μm) were then clamped to the grips, and the extension was measured from the movement of the upper bar. The tensile tests were performed with a load cell of 100 N, crosshead speed of 5 mm min^{-1}, preload of 0.1 N, and gauge length of 20 mm in a Tinnius-Olsen H10KT tensile testing machine (PA). The clamping length was 50 mm. At least 10 specimens were tested for each composition.

Dynamic Mechanical Analysis

Dynamic mechanical thermal analysis (DMTA) was performed with a tensile fixture for films using a Q800 DMA from TA® Instruments at strain amplitude of 3 μm and a fixed frequency of 1 Hz. The temperature ramp was 2°C min^{-1} and the preload tension was 0.01 N. Three strips, 400 μm thick, 5.3 mm wide, and 18 mm long, were cut from each film in the extrusion and the transversal direction to characterize storage modulus (G'), loss modulus (G''), and damping factor (tan δ). The distance between the clamps was set to 12 mm. The temperature range was from 25 to 130°C.

Statistical Analysis

Statistical analysis of the experimental results was performed using Minitab® 16. A general linear model (GLM) was applied to perform an analysis of variance (ANOVA) to identify the most influential factor on essential property responses. Five percent level of significance was considered for further pair-wise comparison of the properties through Tukey post hoc method, unless otherwise, alteration in higher limit for P-value is clearly stated in the report.

RESULTS AND DISCUSSION

Thermogravimetric Analysis

The distribution of the HAp and the fibrous (FCP) respective particle (CP) type cellulose in the bulk of the extruded films was analyzed by TGA analysis of samples taken at different positions along the films. The analysis was done for the films containing 3, 10, and 20 wt % of the FCP respective CP cellulose. The results are shown in Table II, and it can be seen that for all composite films containing cellulose the thermal degradation occurs at a lower temperature compared to the films containing only HAp. This can be expected as cellulose has lower thermal stability than PLA. The degradation temperatures inclusive the standard deviations do not significantly differ for the TGA samples taken at the film edge respective the film middle point. One exception was the film PLA/HAp/CP20, for which the data indicate some inhomogeneity. Humidity uptake by the cellulose in the samples can to some part affect these data. Therefore, the T_5 and T_{80} temperatures are only used to compare the HAp distribution uniformity in the films to assess the consistency of the extrusion process. The char residue in wt % at 700°C is consistent with the HAp loading in the films, although some discrepancy was observed for the PLA/HAp/CP20 film.

Scanning Electron Microscopy

Figures 1 and 2 illustrate the SEM micrographs of cross-sections of the extruded films at low and high magnification, respectively. The PLA/HAp films with particulate cellulose have a fairly good particle distribution as shown in Figure 1(A–D). The PLA/HAp films containing fibrous type cellulose filler show fiber pull-outs and poor fiber orientation, as can be seen in Figure 1(E–H). Their surface morphology is also clearly rough and uneven. This morphology will have an effect on the mechanical properties of the films, as will be discussed later. In the higher magnification micrographs presented in Figure 2 more detailed interpretations can be made. First, strain-hardening is realized in the particulate cellulose-filled composites [Figure 2(A–D)] which is absent in the case of fibrous cellulose-incorporated composites. The white regions pointed out by the arrows in Figure 2(C), increase with the CP concentration up to 10 wt % and disappear at higher loadings, which support the results acquired for tensile yield and elongation at failure of the corresponding composites. Second, it is obvious that the HAp particles are well distributed in both CP and FCP filled composites. Although some hydroxyapatite particle aggregates are formed in the FCP composite, there seems to be fewer aggregates in CP containing composites. Furthermore, random orientation of fibrous cellulose is observed which is not in the axial direction of the extrusion. Fiber pull-out that is seen both for CP and FCP composites is due to poor interfacial adhesion between the cellulose fibers and the matrix.

An encouraging feature of the films is their rough surface topography, essential for cellular interactions.[4] As seen in

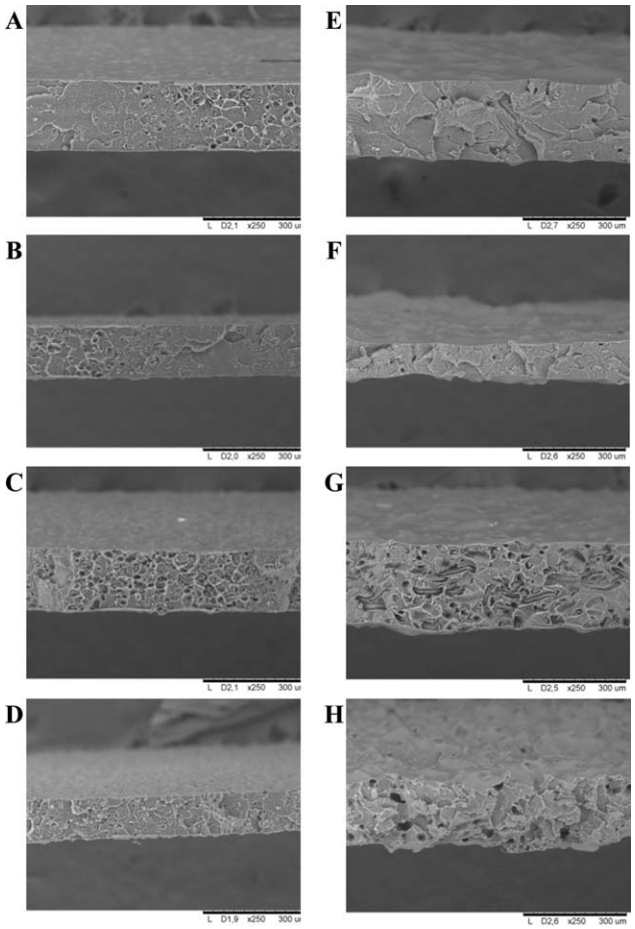

Figure 1. Low magnification scanning electron micrographs of PLA/HAp films containing 3, 5, 10, and 20 wt % particulate cellulose (A–D) and fibrous cellulose (E–H). The length of the scale bare is 300 μm.

Figure 1, the increase in surface roughness by increased fibrous cellulose loading is evident.

Differential Scanning Calorimetry

The thermal characteristics for neat PLA film and the composite films are shown in Table III. The analysis was done to assess the effect of the two different regenerated cellulose types on thermal properties of the PLA matrix. The table gives thermal data obtained from the second heating scan, and for the degree of crystallinity, data from the first heating scan. It is therefore clear that the as-extruded films are almost fully amorphous.

In Figure 3, the differential scanning calorimetry (DSC) scans for neat PLA, PLA with 10 wt % HAp, and PLA with 10 wt % HAp, and 3, 10, and 20 wt % particulate type cellulose are shown. It can be noticed that the glass transition temperature is not affected by the HAp or the CP respective FCP. Efficient dispersion of nanoparticles in a polymer matrix has shown to freeze the mobility of the polymer chains which results in increased glass transition temperature.[31] Same has been reported in another study, the glass transition temperature increased up to 10 wt % nanoparticle loading and reduced upon further increase in the nano/micro-particle content.[32] Therefore, it is likely that aggregated HAp clusters are formed in the made PLA composite films. Consequently, the slight reduction of T_g trend observed in this study can be related to the increased interfacial surface area, resulting in increase of the free volume available for the polymer chains to start moving freely.[33] Furthermore, this is in accordance with the SEM images [see the circles in Figure 2(D–F)] and DMTA results, which will be discussed later. As seen in Table III, due to the fast cooling after extrusion and the thin film thickness, the PLA and the PLA/HAp are fully amorphous. Incorporation of the CP respective FCP cellulose increases the degree of crystallinity as shown by the data for the second heating scan, which indicates the nucleating potential of the cellulose in the PLA matrix.

The glass transition temperature variation for the particulate cellulose modified blends was in agreement with the dynamic mechanical analysis measurements, which are reported below. Table III demonstrates that the fibrous cellulose induce higher degree of crystallinity than the particulate cellulose. Both cellulosic types demonstrate nucleating capacity, which was increased by fiber loading. Although the particulate cellulose has larger surface area available for PLA nuclei formation and growth, it could be possible that the greater crystallinity of the composites with fibrous cellulose could be due to the nucleation potential of the broken and bent regions generated in the long fibrous cellulose during the melt-mixing procedure.[34] This can explain

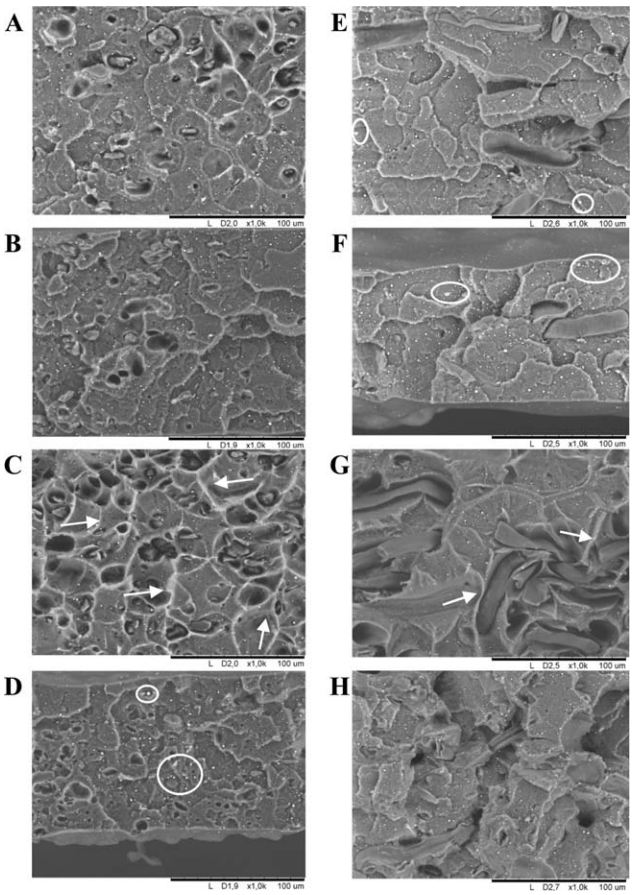

Figure 2. High magnification scanning electron micrographs of films containing 3, 5, 10, and 20 wt % particulate (A–D) and fibrous cellulose (E–H). The length of the scale bare is 100 μm.

Table III. Thermal Properties of the Neat PLA, PLA/HAp, and PLA/HAp Composites Measured by Differential Scanning Calorimetry

Sample	Second heating scan			First heating scan
	ΔH_{mc} (J g^{-1})	ΔH_{RAF} (J g^{-1})	χ (%)	χ (%)
PLA	1.69 ± 0.13	N/A	3.36 ± 0.10	N/A
PLA/HAp	2.86 ± 0.28	N/A	4.88 ± 0.41	N/A
PLA/HAp/CP1	7.46 ± 0.18	0.49 ± 0.03	16.96 ± 1.10	0.62 ± 0.67
PLA/HAp/FCP1	9.11 ± 0.25	0.13 ± 0.02	18.18 ± 0.65	1.10 ± 0.73
PLA/HAp/CP3	4.01 ± 0.61	0.03 ± 0.02	10.36 ± 0.84	0.39 ± 0.21
PLA/HAp/FCP3	4.88 ± 0.21	0.06 ± 0.00	11.46 ± 1.28	0.80 ± 0.77
PLA/HAp/CP5	4.70 ± 0.16	0.01 ± 0.01	9.37 ± 0.47	0.72 ± 0.34
PLA/HAp/FCP5	7.59 ± 0.31	0.57 ± 0.03	17.33 ± 0.71	2.04 ± 1.08
PLA/HAp/CP7	6.46 ± 0.63	0.05 ± 0.02	13.02 ± 0.60	1.59 ± 0.29
PLA/HAp/FCP7	5.01 ± 0.59	0.04 ± 0.01	11.82 ± 0.55	1.20 ± 0.10
PLA/HAp/CP10	7.60 ± 0.06	0.26 ± 0.05	18.08 ± 0.09	1.28 ± 0.25
PLA/HAp/FCP10	10.57 ± 0.11	0.59 ± 0.00	25.26 ± 0.35	4.08 ± 1.66
PLA/HAp/CP15	7.58 ± 0.28	0.23 ± 0.05	18.71 ± 0.47	3.59 ± 0.03
PLA/HAp/FCP15	15.30 ± 0.67	1.06 ± 0.01	32.93 ± 5.01	4.47 ± 0.35
PLA/HAp/CP20	10.95 ± 0.48	0.95 ± 0.02	29.45 ± 0.33	4.19 ± 1.10
PLA/HAp/FCP20	14.03 ± 1.36	0.70 ± 0.03	35.29 ± 5.36	8.36 ± 2.07

The melt-crystallization enthalpy ΔH_{mc}, the rigid amorphous fraction enthalpy ΔH_{RAF}, and the degree of crystallinity χ% obtained from the second heating scan are given. The degree of crystallinity χ% obtained from the first heating scan is given as a comparison. The number in the sample name gives the CP respective FCP content.

their minor effect on the mechanical properties for the films, which will be discussed in the next section.

These results are further supported by the fact that the heat of melt-crystallization has increased at higher fiber content which concomitantly reveals the cellulose reinforcement's capability to induce crystallite-formation resulting in improvement of the crystallinity of HAp-filled polymers. The crystallinity of the PLA/HAp composite films has increased from the rather low value 4% for the films with the thermal history not eliminated (data from first DSC scan) to around 30–40% for the films with the thermal history eliminated (data from second DSC scan), as shown in Table III.

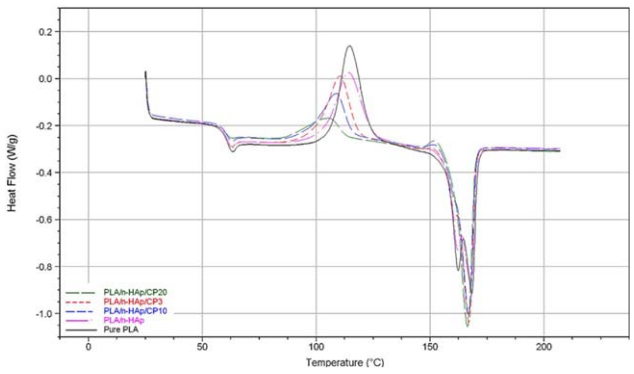

Figure 3. DSC thermograms obtained from second heating cycle of the PLA/HAp composite films reinforced with 3, 10, and 20 wt % particulate cellulose compared with neat PLA and PLA/HAp film. [Color figure can be viewed in the online issue, which is available at wileyonlinelibrary.com.]

The DSC scans in Figures 3 and 4 display an exothermic peak prior to the melting region in HAp/PLA/cellulose composites, which does not exist or is notably small for the PLA/HAp film and the neat PLA films. This is attributed to the crystallization of the rigid amorphous fractions existing at the interface of crystallites and bulk amorphous region. As the crystallinity of the composites increases the share of rigid amorphous fractions is increased, which can re-organize at high temperatures to crystal lamellas, where sufficient energy is available for the PLA chains to start moving freely.[35] The presence of these regions was further supported by a shift to the right for the glass transition temperatures measured during second heating cycle compared with the first heating cycle at all concentrations for both cellulose types.

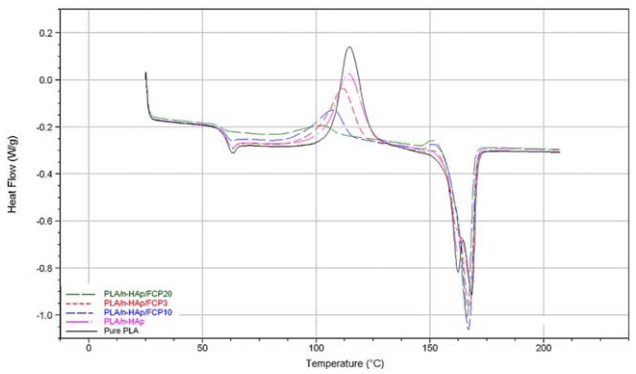

Figure 4. DSC thermograms obtained from second heating cycle of the PLA/HAp composite films reinforced with 3, 10, and 20 wt % fibrous cellulose compared with neat PLA and PLA/HAp film. [Color figure can be viewed in the online issue, which is available at wileyonlinelibrary.com.]

Reduction in the cold-crystallization enthalpy with filler content is in agreement with the other thermal characteristics obtained for the films. This could be explained by the fact that only completely amorphous and mobile PLA chains are able to participate in a spontaneous nuclei generation during cold-crystallization. As the cellulose concentration increase, the likely portion of rigid amorphous fractions develop, leading to low crystallite formation during the heating scan, which were lower than for the PLA/HAp films with approximately 29 J g^{-1}.[35]

As already mentioned, the fibrous and particulate cellulose have nucleating agent capability. It has been claimed that uniform dispersion of nanoparticles and fibrous fillers can hinder crystalline lamella formation by constraining the mobility of the polymer chains.[36] In our case, as the fiber content increase up to 7 wt % the former factor is compromised ending up in declining trend in crystallinities. At 1 wt %, two mechanisms of crystallite generation exist, namely spontaneous spherulite creation in the bulk polymer matrix and single crystal origination from the fibers surface. Based on the hypothesis which will be explained in the DMTA section, a fibrous filler can act as thermal damping medium, therefore, at 1 wt % of cellulose concentrations the relative cooling rate is higher than at other fiber ratios, ending up in many small and imperfect crystals (due to the appearance of double-melting behavior during the fusion stage) in the bulk polymer and around the reinforcements surface. The existence of small crystalline lamellas is verified by the low melting temperature of the corresponding PLA/HAp film. Concerning 3, 5, and 7 wt % fiber content, the relative cooling rate is slower, resulting in the growth of less magnitude but larger crystallites around the fibers, compared to PLA with higher cellulose content, or 1 wt % cellulose.

When the fiber content increase above 10 wt %, it is presumed that a huge amount of single crystals start growing from the filler surface, and due to the relative small free volume available for the crystal growth they impinge to each other, which in turn leads to formation of small and fairly perfect crystalline lamella. This is further supported by narrower width of the melting region of the PLA and fading of the double melting behavior in the composites by fiber content shown in the DSC scans in Figures 3 and 4.

Mechanical Properties

Effect of HAp on PLA. It has been reported that stiff nanofillers show different behavior towards alteration of the composite tensile properties.[37] However, the reinforcing effect might be reduced above a certain filler content. At this point, the nanoparticles start to agglomerate due to poor filler–polymer affinity and further they slip on each other under the applied forces, acting as crack propagation points and eventually lead to reduction in tensile strength.[38,39] The HAp concentration used in this study is supposed to be above the critical amount, therefore, lower mechanical strength is achieved in the PLA/HAp composite compared to neat PLA. The tensile strength, the modulus, and the elongation at break for the made films are shown in Figure 5(A–C). Addition of 10 wt % HAp to PLA has resulted in statistically significant reduction in the tensile strength and yield strength to 54 and 53.7 MPa from approximately 64 and 64.7 MPa for pure PLA, respectively. The elongation at break was not considerably decreased compared to the neat PLA.

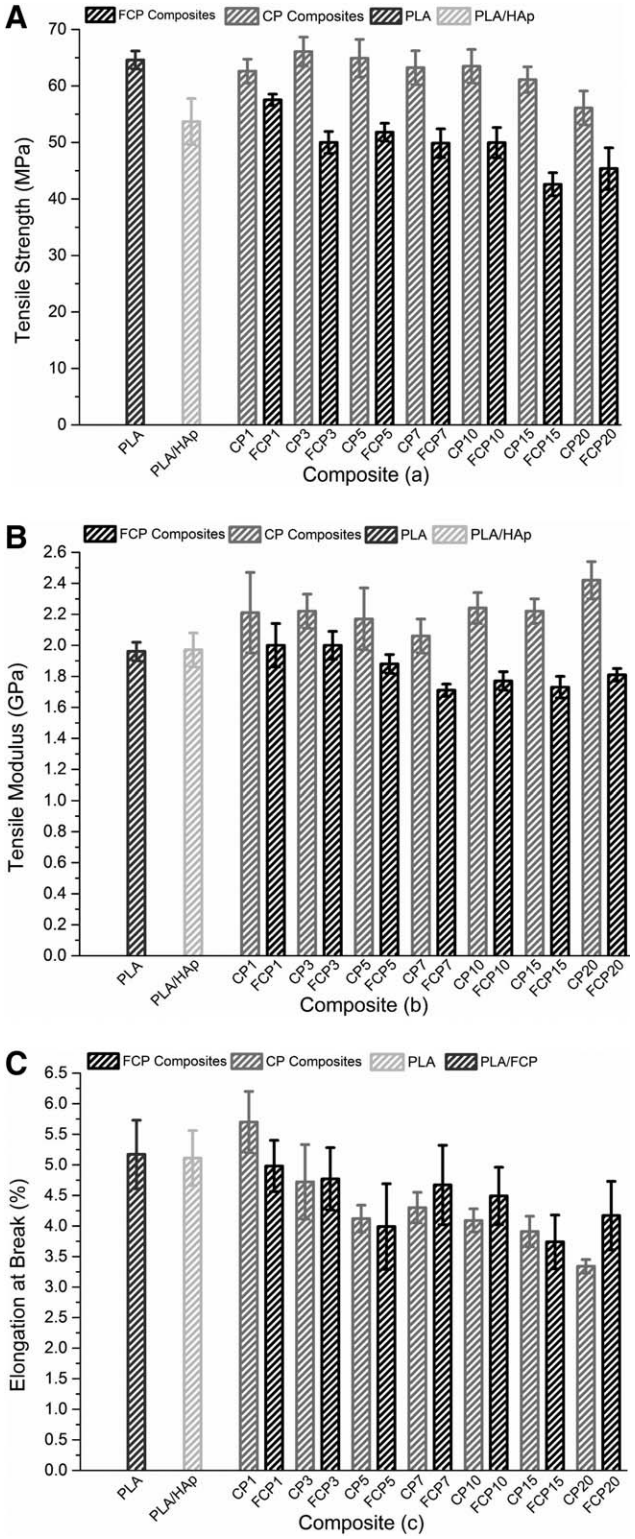

Figure 5. Tensile strength (A), modulus of elasticity (B), and elongation at break (C) for neat PLA (dark gray), PLA/HAp (light gray), and PLA/HAp with particulate (gray) and fibrous (black) cellulose.

To measure the fracture toughness, tensile testing can be performed on specimens with specific crack geometry. In this study, toughness, defined as the amount of energy the material

Table IV. Toughness, Defined as the Total Energy Demand Prior to Rupture Per Unit Volume, for Neat PLA, PLA/Hap, and PLA/HAP Modified with the Particulate Type Cellulose

Sample	Toughness (MJ m^{-3})	*P*-value with respect to pure PLA ($P < 0.05$)	*P*-value with respect to PLA/HAp ($P < 0.05$)
PLA	2.05 ± 0.32	-	-
PLA/Hap	1.75 ± 0.26	0.0115	-
PLA/HAp/CP1	2.26 ± 0.71	0.7115	0.0018
PLA/HAp/CP3	1.91 ± 0.35	0.9872	0.9579
PLA/HAp/CP5	1.47 ± 0.15	0.0016	0.4736
PLA/HAp/CP7	1.58 ± 0.15	0.0598	0.9579
PLA/HAp/CP10	1.44 ± 0.16	0.0026	0.4543
PLA/HAp/CP15	1.37 ± 0.11	0.0003	0.1570
PLA/HAp/CP20	1.10 ± 0.07	0.0000	0.0001

absorbs per unit volume before rupturing,[40] was numerically calculated as the surface area under the corresponding stress–strain curves. The obtained values are presented in Table IV. This data are used to compare the toughness for the various compositions; the intention was not to provide absolute values for fracture toughness. It can be seen that the toughness was reduced when HAp was added to the neat PLA. The toughness is highly sensitive to the elongation at break, however, a dramatic reduction in tensile strength of around 16% in the case of the PLA/HAp compared to neat PLA films weighed down the positive effect of unchanged elongation at failure for the former with respect to pure PLA.

Concerning the tensile modulus, a 10 wt % HAp loading did not result in the wanted stiffness enhancement, mainly due to the non-uniform distribution of the HAp particles during the manufacturing process. This is further approved by significant attenuation of the toughness in the HAp/PLA film with respect to pure PLA films, as shown in Table IV. Damadzadeh et al. reported the same behavior for HAp with a particle size less than 200 nm incorporated into PLA.[32]

Effect of Cellulose Loading on PLA/HAp Composites. The Young's modulus is measured at low deformations, until almost no separation between the filler and matrix occurs and therefore, it is reasonable to assume that the composite stiffness is independent of the interfacial adhesion between the PLA matrix and the HAp particles.[37] In the case of PLA/HAp films, modified with the fibrous type cellulose, the filler's irregular orientation at the composites' cross-section (apparent in the SEM images in Figure 1), concealed the stiffening potential of the fibrous type cellulose. It can be seen that the undesirable impact of these factors gets severe as the fiber content is increased and Young's modulus decrease from 2 GPa for composite with 3 wt % FCP to 1.8 GPa for the composite with 20 wt % FCP, which contradicts previously reported results.[41] This is also likely to be the consequence of the interference of the long fibers with perpendicular orientation of the crystallite lamella planes with respect to machining direction.[42]

Because of the solvent dissolving and freeze granulation method used to prepare the composites, the cellulose is well dispersed, with very low aggregation even at high loadings. Further, particulate cellulose has higher stiffness compared to the polymer matrix and it does not deform severely consequently, it restricts the PLA molecular chains to move and slide on each other freely.[43] The overall outcome is enhancement of the mean modulus from 1.97 GPa for the PLA/HAp film to 2.42 GPa for 20 wt % particulate cellulose loaded PLA/HAp films.

Proper stress transfer between the particulate respective fibrous fillers and the polymer matrix is a crucial factor in determination of the composites' tensile strength. Discontinuity in the matrix due to weak filler–matrix interfacial adhesion and ineffective stress transfer between the two phases results in decreased strength, which becomes worse by higher filler loading. In Figure 2 [e.g., Figure 2(C,G)], voids are seen in the close vicinity of the fibrous and particulate cellulose, these voids are obviously due to poor interfacial adhesion. Thus, the tensile strength attenuates, particularly in the case of composites with fibrous type cellulose, compared to the neat PLA, as shown in Figure 5. Another reason for the voids could be residual solvent from the solvent blending or absorbed humidity after granulation. The former's likelihood is very small as freeze- and oven-drying of the samples were done for sufficient time. Absorbed humidity is a more likely explanation, and in the TGA analysis it was also seen that a minor weight loss occurred around 100°C.

It is well established that increase in polymer crystallinity makes the material brittle and adversely affects the elongation at failure, but not necessarily the elastic strain (i.e., the initial part of the stress–strain curve).[44] Presumably, in the cellulose reinforced composites the synergistic deteriorating effect of voids and defects formed around the fibers and the enhanced crystallinity by reinforcement content result in degradation of elongation at failure with regard to the neat PLA films and the PLA/HAp films. This tendency is highlighted for the composites with fibrous cellulose.

Thermal history is of great importance considering the polymer–filler interfacial fate. Transcrystalline regions between the crystallite lamella of the matrix and the fillers may act as load-transferring regions.[45] Nonetheless, it is clear that even with improved crystallinity by increasing the cellulose content, intensified effect of the trace transcrystalline zones could not overcome the weakening weight of the poorly adhered fiber–matrix areas. This declining trend observed for fibrous cellulose filled composites match the results reported for bleached kraft pulp with smooth surfaces incorporated in PLA matrix.[46] Even though in comparison with pure PLA films considerable improvement in tensile strength is not achieved by the added reinforcement, the tensile strength has not dropped considerably up to 15 wt % in the case of particulate cellulose. As shown in Figure 5, a mean tensile strength of 66 MPa has been obtained for PLA/HAp/CP3, which is non-significantly higher than the value measured for neat PLA thin films.

Statistical analysis shows the significant enhancement in tensile strength of the PLA/HAp composite by addition of the

particulate cellulose at 1% level of significance ($P < 0.01$). Up to 15% cellulose concentration in the PLA/HAp/CP composites improved the tensile strength compared to the PLA/HAp films. This is noticeable for the 3 wt % particulate cellulose composite with approximately 13 MPa gain in mean value compared to 54 MPa for the PLA/HAp composite.

From a micromechanical point of view, our observations somewhat contradict some of the reported results regarding the effect of the residual thermal stresses—caused by the difference in thermal expansion coefficients of the fiber and polymer matrix in fiber composites during the cooling process—on the consequent residual compressive and longitudinal stress built up in the fiber and the matrix, respectively.[47,48] We suppose that the high cooling rate used in the film extrusion hindered the composites from having anneal-like shrinkage of the PLA matrix and consequently high-crystallinity composites, as seen in Table III. In other words, the process dispossessed the composites from thermal expansion coefficient differences, which could induce compressive residual stresses and remarkably improve the interfacial stress transfer and consequently raise the tensile strength for all made composites.[49] Therefore, careful attention should be paid to the production process itself so as to achieve higher mechanical properties, specifically tensile strength.

Here, it is presumed that although the fibrous cellulose modifies the composite crystallinity, it hinders the directional organization of the polymer matrix lamella (preferably perpendicular to machining direction), even at low concentrations. Thus, attenuation in tensile strength and elongation at failure with regard to neat PLA and PLA/HAp composite with yield strength values of 64.6 respective 53.7 MPa is simply predictable.[50]

The discussion provided in this section support the conclusion that the reduction in tensile strength and elongation at break of the fibrous cellulose filled composites in comparison with the PLA/HAp composites is significant ($P < 0.05$).

Crazing Effects in the Composites. The calculated toughness results for the fibrous cellulose filled composites are ignored, as the toughness values were much lower than those of neat PLA, as it can be realized from the data in Figure 5.

In the glassy state, the main yielding process is due to crazing, not due to shear yielding. The craze zone is composed of many highly oriented fibrils, which endow high stress-carrying capacity to the material, as the covalent bonds in the fibrils are much stronger than the secondary van der Waals bonds. Up to 10 wt % CP concentration, the composite toughness increased, compared to neat PLA films and PLA/HAp (Table IV).[40]

As it can be seen in the SEM images [Figure 2(A–C)] corresponding to 3, 5, and 10 wt % particulate cellulose composites, the white lines are indicative of stress-whitening occurrence at regions between the cellulose particulates due to lamella separation and multiple crazing occurrence.[50] At low particulate cellulose content, based on the SEM micrographs, the polymer interface debonding of the partially rigid cellulose particles support appearance of multiple crazing, ending up with satisfactory toughness (Table IV).[42] By even better particulate dispersion in the composite cross-section, the post-distributed stresses caused by neighboring fibrils right after the primary fibril rupture will be stabilized and so, internal flexural momentum appeared due to non-uniform stress distribution is prevented (note the step-like sharp edges shown in the SEM micrographs of particulate cellulose filled composites in Figure 1). Thus, superior plastic behavior could be obtained for the particulate cellulose filled PLA compared to neat PLA.

Dynamic Mechanical Analysis

The results from the DMTA analysis presented in Table V show that there is no effect on the storage modulus at 10 wt % HAp loading compared to neat PLA. This indicates that the HAp–PLA interfacial adhesion is not strong. The balance between stiffening effect of the rigid HAp particles and the available interfacial surface area between the particles and the matrix has probably led to dominant particle agglomeration. The storage modulus at 37°C obtained in this study for the PLA/HAp is much higher than to the values reported for PLGA- and PLLA–HAp based nanocomposites.[33,51]

The storage modulus of the composites at temperatures above the T_g (i.e., 70°C) is presented in Table V to demonstrate the percolating effect in the composites. The temperature for the tan δ peak was around 68–70°C, which is higher than the T_g values obtained from DSC (around 61°C), at this temperature the storage modulus increases from 14.4 MPa for the neat PLA to 16.4 MPa for the 10 wt % HAp/PLA. As the as-extruded neat PLA and PLA/HAp films are both amorphous, the percolating behavior of the filler at temperatures close to the T_g results in higher elastic performance of the PLA/HAp compared to neat PLA.[51]

Viscoelastic properties of composite materials are dependent on the matrix structural and physico-mechanical properties; therefore, shifts in the position of tan δ peak would mainly be the result of filler–matrix interactions at molecular level, which in turn can delay or speed up the onset of polymer chains mobility. Conversely, tan δ peak value can be altered by the physical inhibitory effect of the fillers incorporated in the amorphous regions.[52] An efficient matrix–filler interfacial sliding friction, which seems to be higher in particulate cellulose composites with larger interfacial surface area, releases the absorbed energy.[50] The likelihood of highly agglomerated fibrous cellulose formation in the composites can reduce the polymer chain mobility, which has led to the superior storage modulus for the composites close to T_g. An additional explanation is their more effective performance as stress carrier than for the particle type cellulose. Thus, the former phenomena dominates in the PLA filled with the particulate cellulose, and results in slightly higher loss factor, while the latter factors are responsible for higher storage modulus at 70°C of composites aimed to reinforced with fibrous cellulose.[53] As the cellulose loading increase, the stress will be primarily carried by the filler and less energy is used to strain the interface which eventually dissipates as inter-friction energy between the polymer matrix molecular chains, ending up in attenuation of tan δ peak by the added cellulose filler.[54]

As the composite fiber content increases the stress distribution in the composite cross-section become uniform resulting in

Table V. Storage Modulus G' Measured in the Extrusion Direction at 37°C and 70°C for the Neat PLA, PLA/HAp, and PLA/HAp Cellulose Composite Films

	Extrusion direction					Transversal direction	
Composite	G' at 37°C (MPa)	sd	G' at 70°C (MPa)	stdv	tan δ height	G' at 37°C (MPa)	stdv
PLA	3195	119	14.4	1.1	3.02		
PLA/HAp10	3298	159	16.4	0.2	2.98		
PLA/HAp10/CP1	3523	110	17.9	3.7			
PLA/HAp10/CP3	3372	207	18.6	3.5		2922	7
PLA/HAp10/CP5	3277	299	18.5	3.6			
PLA/HAp10/CP7	3485	110	22.8	1.5			
PLA/HAp10/CP10	3555	60	19.3	4.2		2709	28
PLA/HAp10/CP15	3636	178	25.1	4.1			
PLA/HAp10/CP20	3403	130	22.4	1.2		2474	1
PLA/HAp10/FCP1	3166	75	21.1	0.7			
PLA/HAp10/FCP3	3219	41	18.9	4.7		2710	24
PLA/HAp10/FCP5	3146	687	19.9	4.5			
PLA/HAp10/FCP7	3207	104	23.8	3.8			
PLA/HAp10/FCP10	3309	34	30.2	12.0		2365	32
PLA/HAp10/FCP15	3037	76	44.1	3.1			
PLA/HAp10/FCP20	3398	56	50.6	6.1		1959	65

stdv = standard deviation.
The tan δ height associated with neat PLA and PLA/HAp and the storage modulus G' at 37°C in the transversal direction for PLA/HAP with 3, 10, and 20 wt % particulate and fibrous cellulose are also given.

improvement of storage modulus and/or stiffness at temperatures far lower than T_g.[52] The storage modulus values for the composites presented in Table V show enhanced elastic energy absorption as compared to those of neat PLA and PLA/HAp composite. The higher storage modulus achieved by the particulate cellulose-filled PLA at 37°C is in line with the results obtained from tensile tests and is attributed to the well dispersion of the particles in the composite. For the fibrous cellulose-filled composites, the lack of proper fiber distribution and inefficient alignment of the fibers in the testing direction have led to unsatisfactory stiffness. It is presumed that high particulate cellulose content up to 20 wt % results in formation of hydrogen bonds between cellulosic fibers, which leads to their scattered agglomeration. Therefore, the storage modulus slightly decreases from 3523 to 3372 MPa when the particulate cellulose content is increased from 1 to 5 wt %. The storage modulus reaches its highest value (3636 MPa) for the 15 wt % particulate cellulose containing composite, which is the only composition with statistically significant modulus enhancement compared to neat PLA films (P-value = 0.0377 < 0.05). A quite similar tendency can also be recognized in the E-modulus from the tensile testing [Figure 5(B)].

Data presented in Table V demonstrate improvements in the storage modulus at 37 and 70°C for the particulate cellulose composites compared to the PLA/HAp films. These superior properties are evident for PLA/HAp/CP15% with 3636 and 25 MPa as compared with 3298 and 16.4 MPa obtained for the PLA/HAp film.

The storage modulus at 37°C in the transversal direction is significantly lower than in the extrusion direction as shown in Table V. The difference is greater at higher cellulose content, but smaller for the particulate cellulose filled PLA-composites due to their symmetrical morphology. In the transversal direction, the storage modulus at 37°C for all tested composites is lower than the storage modulus for neat PLA films which could indicate that the main part of the fibrous cellulose is oriented in the extrusion direction and consequently will not improve the storage modulus in the transversal direction. However, this argumentation is contradicted by the SEM results for the fibrous cellulose composites, as discussed earlier. Therefore, it is expected that by further controlling the orientation of the fibrous cellulose at higher contents, a superior storage modulus in the extrusion direction can be achieved for the PLA/HAp filled with the fibrous cellulose. It is noteworthy that the deteriorating effect of PLA chain alignment on the storage moduli in the transversal direction is neglected for both types of cellulose composites while providing the following discussion. Although the used CP cellulose is claimed to have particulate-shape, the viscoelastic characteristics of their composites show anisotropic performance, which could be associated with either their longitudinal deformation in the extrusion direction during melt-mixing process or particle aggregation. The forces involved in the extrusion process are unlikely to deform the fillers. Regarding the latter probable cause of anisotropic behavior of the composites T_gs obtained by tangent construction in DMTA analysis can be more reliable on clarifying the formation of aggregates. This anisotropic behavior has been shown to be

favorable for bone substitute biomaterials due to the anisotropic complex nature of the natural bone itself.[15]

A simple method to investigate the presence of various damping mechanisms in a composite is to validate the following relationship. If the damping mechanism in the composite is similar to the pure polymer matrix, the following hypothetical relation should be held[55]:

$$V_p = \tan \delta_r = \frac{\tan \delta_c}{\tan \delta_p}. \quad (2)$$

V_p, tan δ_c, tan δ_p, and tan δ_r are the volume fraction of the polymer matrix in the composite, damping factor of the composite and the neat PLA film, and the relative damping ratio at a particular temperature, respectively. The difference in glass transition temperatures reported for all tested composites is not remarkable (providing the results associated with glass transition temperatures of the ternary composites presumed redundant). Therefore, it is worth investigating the impact of the fillers on the damping characteristics of the composites at two representative temperatures below and above the neat PLA glass transition temperature of approx. 62°C, namely 37 and 72°C. Corresponding values to the theoretical formulation and the experimental data achieved via DMTA measurements at these two temperatures are shown in Table V. In addition, the trends are illustrated in Figure 6.

If at temperatures higher than T_g, the experimentally calculated ratios demonstrate ascending trend by decline in PLA volume fraction, a conflict seems to happen. As the portion of highly restricted amorphous region increases by the filler content as it was described earlier, the energy absorption performance of the composite should augment as the crystallinity enhances and polymer matrix volume fraction reduces by reinforcement content. In another word, a descending trend is expected because of the decrease in matrix volume fraction; however, this is not the case for both CP and FCP ternary composites. This conveys the existence of other damping procedures, such as frictional losses at the filler–matrix and filler–filler interface due to the appearance of small agglomerates in the composite, which overwhelms the elastic behavior imposed by the highly organized and restricted PLA chains.[55]

At temperature above T_g and at low cellulose contents although the polymer volume fraction is high, the restrictive effect of the cellulosic reinforcements dominates. This is more pronounced with FCP than CP as the corresponding relative tan δ is far below the theoretical values, probably due to interlocking of the fibers. As the reinforcement loading increased, the defined damping ratio inclined concurrently and leveled out the theoretically calculated PLA volume fraction at 20 wt % FCP and 15 wt % CP content. This illustrates the mount in severity of energy dissipation modes by the reinforcement content as discussed in the previous paragraph which is more emphasized for the PLA/HAp/CP composites.

The relative damping factor for the PLA/HAp composite was far higher than the cellulose containing composites at 72°C. This illustrates the effectiveness of the cellulosic reinforcements

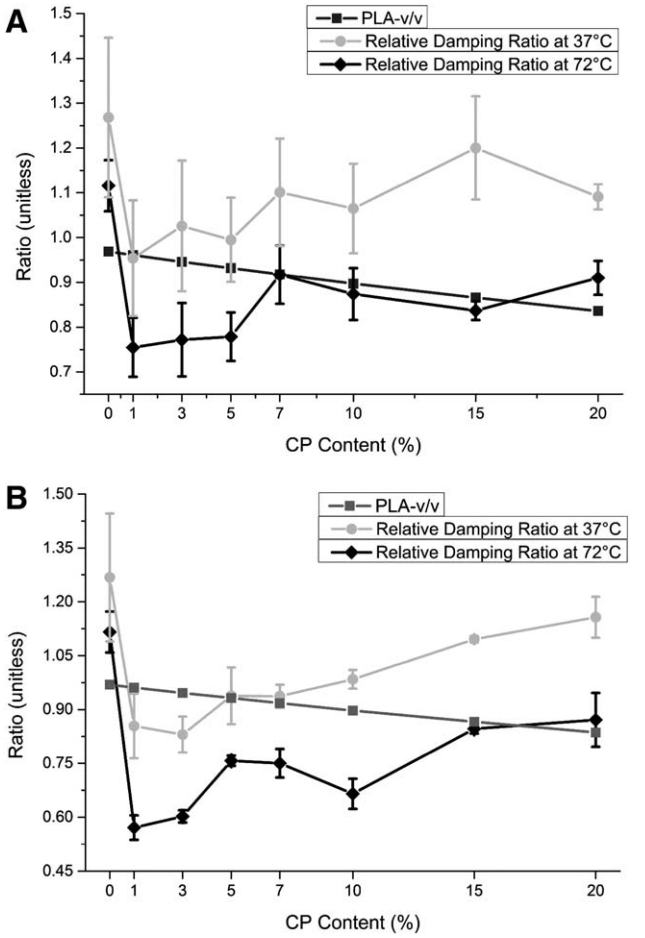

Figure 6. PLA volume fraction and relative damping ratio of (A) PLA/HAp and PLA/HAp/CP and (B) PLA/HAp and PLA/HAp/FCP film composites at temperatures below (37°C) and above (70°C) the T_g for the PLA matrix (~62°C).

in the reduction of released energy proportion from the total absorbed energy by for instance, lowering the relative decline in energy absorption with regard to energy loss as heat (Figure 6).

At temperatures below T_g namely, 37°C, results presented in Figure 6 (and Table II) prove the ascending trend by fibrous cellulose loading. In the particulate cellulose composites, the damping capacity has not changed significantly by particle loading. Nevertheless, the ratio is larger than the volume fraction of the PLA matrix composites at almost all the compositions, which is an evidence for the existence of rigorous damping mechanisms such as interfacial friction and filler–filler frictional losses. General Linear Model with the cellulose type and content as the main factors, demonstrated the considerable effect of CP on enhancement in the relative damping ratio ($P < 0.01$). The PLA/HAp reinforced with CP also did not show significant reduction of the relative damping ratio in comparison with the PLA/HAp composites. Consequently, shock absorption efficiency of the particulate cellulose-reinforced composites was enhanced with regard to the biomaterials reinforced with fibrous cellulose and remained constant with regard to PLA merely filled with HAp.

The viscoelastic properties of the made composites falls below the real cortical bone values (*ca.*, 8 GPa)[56] and it is far higher than values ascribed to cancellous bone (50–500 MPa).[33] However, 30–90% porosity of the cancellous bone mimetic substitutes should not be neglected.[21] It is worth mentioning that the damping capacity of the CP-reinforced PLA nanocomposite is higher than rigid FCP-reinforced nanocomposites at all the compositions.

CONCLUSIONS

The aim with this study was to investigate the effect of regenerated particulate or fibrous cellulose on the mechanical and thermal properties for hydroxyapatite modified PLA films. PLA/HAp/cellulose blends were produced by a solvent mixing technique, which gave a composite granulates which easily could be extruded to homogeneous films. An expected result was that by introducing 10 wt % of HAp nanoparticles into PLA, the dynamic thermomechanical and tensile properties of the composite degrades. However, when regenerated cellulose was added to the PLA/HAp composite the thermal and mechanical properties could be improved. The effect was especially pronounced when particulate type cellulose was added to the PLA/HAp composites.

The best storage modulus enhancement achieved for the PLA/HAp cellulose composites was for composites with 15 wt % particulate type cellulose. The improvement was 14% when compared to neat PLA and 10% when compared PLA/HAp. By addition of up to 15 wt % particulate cellulose, the yield strength was significantly increased, whereas 23% augmentation in ultimate tensile strength was realized by 3 wt % particulate cellulose compared to PLA/HAp.

The PLA/HAp films with the fibrous cellulose performed better at temperatures above T_g, ending up in higher storage modulus, which could be due to aggregated and entangled fibers which above the glass transition temperature could prevent deformation of the softened amorphous part of the matrix. Higher matrix crystallinities were observed for the PLA/HAp composites with fibrous cellulose compared to the composites with particulate cellulose, which could be due to the easier aggregation of the latter type. However, due to the lack of entanglement for the particulate cellulose aggregation, these did not enhance modulus and tensile strength at 37°C, which corresponds to the physiological temperature. It would be necessary to do TEM analysis on the composites, to verify these assumptions.

Further research is needed to evaluate the capability of cellulosic fibers for appropriate dispersion of HAp, which should be beneficial in the case of preosteoblast cells differentiation into osteoblasts.[4] Moreover, better distribution of the HAp can strengthen its osteoconductivity characteristics in the implanted scaffold.

Eventually, it is believed that cellulosic micro-particles can remarkably upgrade mechanical properties, energy storage, and damping capacity of biomedically applicable HAp filled composites, alter their surface topography, disperse bioactive nanoceramics uniformly in the constitutive scaffold composites and perhaps improve their hydrophilicity, all demanded characteristics of a prospective candidate for bone tissue engineering applications.

ACKNOWLEDGMENTS

Laboratory technician Haike Hilke is gratefully acknowledged for the help during the experimental work.

REFERENCES

1. Canal, C.; Ginebra, M. P. *J. Mech. Behav. Biomed. Mater.* **2011**, *4*, 1658.
2. Gupta, B.; Revagade, N.; Hilborn, J. *Prog. Polym. Sci.* **2007**, *32*, 455.
3. Armentano, I.; Dottori, M.; Fortunati, E.; Mattioli, S.; Kenny, J. M. *Polym. Degrad. Stab.* **2010**, *95*, 2126.
4. Liu, X.; Holzwarth, J. M.; Ma, P. X. *Macromol. Biosci.* **2012**, *12*, 911.
5. Puppi, D.; Chiellini, F.; Piras, A. M.; Chiellini, E. *Prog. Polym. Sci.* **2010**, *35*, 403.
6. Swetha, M.; Sahithi, K.; Moorthi, A.; Srinivasan, N.; Ramasamy, K.; Selvamurugan, N. *Int. J. Biol. Macromol.* **2010**, *47*, 1.
7. Lim, L. T.; Auras, R.; Rubino, M. *Prog. Polym. Sci.* **2008**, *33*, 820.
8. Müller, F. A.; Müller, L.; Hofmann, I.; Greil, P.; Wenzel, M. M.; Staudenmaier, R. *Biomaterials* **2006**, *27*, 3955.
9. Averous, L. *Macromol. Chem. Phys.* **2009**, *210*, 890.
10. Carrillo, F.; Colom, X.; Cañavate, X. *J. Reinf. Plast. Compos.* **2010**, *29*, 359.
11. Pooyan, P.; Tannenbaum, R.; Garmestani, H. *J. Mech. Behav. Biomed. Mater.* **2012**, *7*, 50.
12. Entcheva, E.; Bien, H.; Yin, L.; Chung, C.-Y.; Farrell, M.; Kostov, Y. *Biomaterials* **2004**, *25*, 5753.
13. Bose, S.; Tarafder, S. *Acta Biomater.* **2012**, *8*, 1401.
14. He, M.; Chang, C.; Peng, N.; Zhang, L. *Carbohydr. Polym.* **2012**, *87*, 2512.
15. Cai, X.; Tong, H.; Shen, X.; Chen, W.; Yan, J.; Hu, J. *Acta Biomater.* **2009**, *5*, 2693.
16. Goetz, L.; Mathew, A.; Oksman, K.; Gatenholm, P.; Ragauskas, A. *J. Carbohydr. Polym.* **2009**, *75*, 85.
17. Gouma, P.; Xue, R.; Goldbeck, C. P.; Perrotta, P.; Balázsi, C. *Mater. Sci. Eng., C* **2012**, *32*, 607.
18. Wei, G.; Ma, P. X. *Biomaterials* **2004**, *25*, 4749.
19. Habibovic, P.; Barralet, J. E. *Acta Biomater.* **2011**, *7*, 3013.
20. Ulery, B. D.; Nair, L. S.; Laurencin, C. T. *J. Polym. Sci., Part B: Polym. Phys.* **2011**, *49*, 832.
21. Wagoner Johnson, A. J.; Herschler, B. A. *Acta Biomater.* **2011**, *7*, 16.
22. Holzwarth, J. M.; Ma, P. X. *Biomaterials* **2011**, *32*, 9622.
23. Liao, X.; Lu, S.; Zhuo, Y.; Winter, C.; Xu, W.; Li, B.; Wang, Y. *Cell. Mol. Bioeng.* **2011**, *4*, 579.
24. Zhou, Z. *J. Macromol. Sci. Part B* **2007**, *46*, 1247.
25. Lin, N.; Huang, J.; Chang, P. R.; Feng, J.; Yu, J. *Carbohydr. Polym.* **2011**, *83*, 1834.
26. Way, C.; Dean, K.; Wu, D.; Palombo, E. *J. Polym. Environ.* **2011**, *19*, 849.

27. Huda, M. S.; Mohanty, A. K.; Drzal, L. T.; Schut, E.; Misra, M. *J. Mater. Sci.* **2005**, *40*, 4221.
28. Solarski, S.; Ferreira, M.; Devaux, E. *Polymer* **2005**, *46*, 11187.
29. Fortunati, E.; Armentano, I.; Zhou, Q.; Iannoni, A.; Saino, E.; Visai, L.; Berglund, L. A.; Kenny, J. M. *Carbohydr. Polym.* **2012**, *87*, 1596.
30. Carrasco, F.; Pagès, P.; Gámez-Pérez, J.; Santana, O. O.; Maspoch, M. L. *Polym. Degrad. Stab.* **2010**, *95*, 116.
31. Kalfus, J.; Jancar, J. *Polym. Compos.* **2007**, *28*, 365.
32. Damadzadeh, B.; Jabari, H.; Skrifvars, M.; Airola, K.; Moritz, N.; Vallittu, P. *J. Mater. Sci. Mater. Med.* **2010**, *21*, 2523.
33. Wilberforce, S. I. J.; Finlayson, C. E.; Best, S. M.; Cameron, R. E. *Polymer* **2011**, *52*, 2883.
34. Kowalczyk, M.; Piorkowska, E.; Kulpinski, P.; Pracella, M. *Composites Part A* **2011**, *42*, 1509.
35. Delpouve, N.; Saiter, A.; Dargent, E. *Eur. Polym. J.* **2011**, *47*, 2414.
36. Zhang, Q.; Mochalin, V. N.; Neitzel, I.; Hazeli, K.; Niu, J.; Kontsos, A.; Zhou, J. G.; Lelkes, P. I.; Gogotsi, Y. *Biomaterials* **2012**, *33*, 5067.
37. Fu, S.-Y.; Feng, X.-Q.; Lauke, B.; Mai, Y.-W. *Composites Part B* **2008**, *39*, 933.
38. Garoushi, S.; Lassila, L.; Vallittu, P. *J. Mater. Sci. Mater. Med.* **2011**, *22*, 1645.
39. Yan, L.; Shaoyun, F.; Dajie, L.; Yihe, Z.; Qinyan, P. *Fuhe Cailiao Xuebao (Acta Mater. Compos. Sin.)* **2005**, *22*, 11.
40. Anderson, T. L.; Fracture Mechanics: Fundamentals and Applications; Taylor & Francis Group: USA, **2005**; Vol. 6, p 257.
41. Wang, M.; Berry, C.; Braden, M.; Bonfield, W. *J. Mater. Sci. Mater. Med.* **1998**, *9*, 621.
42. Cotterell, B.; Chia, J. Y. H.; Hbaieb, K. *Eng. Fract. Mech.* **2007**, *74*, 1054.
43. Mahmoudian, S.; Wahit, M. U.; Ismail, A. F.; Yussuf, A. A. *Carbohydr. Polym.* **2012**, *88*, 1251.
44. Chen, Q.; Liang, S.; Thouas, G. A. *Prog. Polym. Sci.* **2012**, *38*, 584.
45. Le Duigou, A.; Davies, P.; Baley, C. *Compos. Sci. Technol.* **2010**, *70*, 231.
46. Iwatake, A.; Nogi, M.; Yano, H. *Compos. Sci. Technol.* **2008**, *68*, 2103.
47. Wagner, H. D.; Nairn, J. A. *Compos. Sci. Technol.* **1997**, *57*, 1289.
48. Nairn, J.; Zoller, P. *J. Mater. Sci.* **1985**, *20*, 355.
49. Parlevliet, P. P.; Bersee, H. E. N.; Beukers, A. *Composites Part A* **2006**, *37*, 1847.
50. Sperling, L. H.; Introduction to Physical Polymer Science; Wiley, **2006**; Vol. 11, p 557.
51. Wilberforce, S.; Best, S.; Cameron, R. *J. Mater. Sci. Mater. Med.* **2010**, *21*, 3085.
52. Kiziltas, A.; Gardner, D. J.; Han, Y.; Yang, H.-S. *Thermochim. Acta* **2011**, *519*, 38.
53. Suhr, J.; Koratkar, N. A.; Ye, D.; Lu, T.-M. *J. Intell. Mater. Syst. Struct.* **2006**, *17*, 255.
54. Sim, K. J.; Han, S. O.; Seo, Y. B. *Macromol. Res.* **2010**, *18*, 489.
55. Bleach, N. C.; Nazhat, S. N.; Tanner, K. E.; Kellomäki, M.; Törmälä, P. *Biomaterials* **2002**, *23*, 1579.
56. Wang, T.; Feng, Z. *Mater. Lett.* **2005**, *59*, 2277.